CAUCHY MACHINE FOR BLIND INVERSION IN LINEAR SPACE-VARIANT IMAGING

Harold Szu and Ivica Kopriva
Digital Media RF Lab, ECE Department, George Washington University
725 23rd St. NW, Washington DC 20052, USA
e-mail: ikopriva@seas.gwu.edu; SZUH@onr.navy.mil

Abstract - We revisited Cauchy Machine for solving blind space-variant imaging problem on the pixel by pixel basis. Under-determinacy of the pixel by pixel blind-matrix inversion was accomplished non-statistically by a physics-constraint of open information systems in a dynamic balance by minimizing the thermodynamics free energy $H=U-T_0S$ where U is estimation error energy, T_0 is temperature and S is the entropy. Solution was found through algorithm that computes the unknown source vector and unknown mixing matrix using Cauchy Machine to find the global minimum of H for each pixel. We demonstrated the algorithm capability to perfectly recover images from the noise free linear mixture of images. Capability of the Cauchy Machine to find the global minimum of the 'golf hole' type of landscape has been demonstrated in higher dimensions with a less computation complexity than an exhaustive search algorithm.

I. INTRODUCTION

Ackley, Hinton & Sejnowski [1] had developed Boltzmann Machines and demonstrated on a supercomputer in a several days to generate the "Net-talk" of a child pronunciation. Geman & Geman [2] had proved that simulated annealing algorithm based on Boltzmann thermal noise would require a slow cooling schedule inversely proportional with the logarithm of the time steps. Szu et al. [3,4] had proved that Cauchy color noise, rather than Boltzmann thermal noise, could achieve the global optimization in a much faster cooling schedule that is inversely proportional with the time steps. Important novelty of this paper is implementation of the 2D Cauchy machine to find the global minimum of the 'golf hole' type of landscape that arises in deterministic blind inversion of the space-variant imaging problems, Szu and Kopriva [5,6], right side on Figure 1. In the 'ocean' type landscape, left side on Figure 1, the single minimum can be found by ordinary deterministic gradient descent algorithm. However, constrained optimization problems very often result in multiple minimums with the 'lake' type of landscape, middle of the Figure1, or 'golf hole' type of landscape, right side of the Figure 1. For such cases the gradient descent algorithm will be trapped in some of the local minimums. Stochastic search based on simulated annealing theory [1-4] enables non-convex optimization algorithm to escape from the local minima. It has been proven that convergence of the stochastic search based on the Cauchy distribution with unbounded variance (Cauchy Machine), [3,4], is inversely proportional with time while convergence of the stochastic search algorithms based on Gaussian distribution (Boltzmann Machine), [1], is inversely proportional with the logarithmic function of time [2]. Convergence of the Cauchy Machine has been demonstrated in [4] for a 1D double-well potential function and the 2D equivalent of which is shown in the middle of the Figure 1 (the 'lake' type of landscape). The Helmholtz free energy based objective function used in blind space-variant imaging problems, [5,6], has from the global optimization point of view a very difficult 'golf hole' type of landscape, right side on Figure 1.

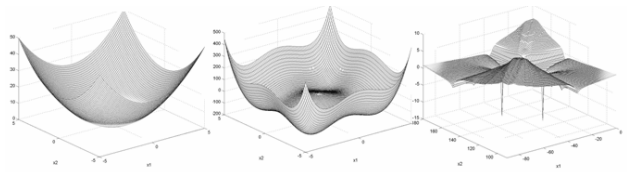

Figure 1. From left to right are 2D objective functions with ocean like landscape; multiple lakes like landscape; golf hole like landscape.

We demonstrate in this paper, according to our knowledge for the first time, application of the 2D Cauchy Machine on the global minimization of the 'golf hole' type of landscape which comes from the real world constrained optimization problem such as blind de-mixing of the space-variant mixture of images, [5,6]. New solution for deterministic blind space-variant imaging problem is proposed as a marriage of the unsupervised feed-forward type of the Lagrange Constraint Neural Network (LCNN), [7,5,6], Figure 2, and 2D Cauchy Machine, [3,4]. Unlike statistical independent component analysis (ICA) algorithms [8,9,10] solution is deterministic and solves the problem on the pixel by pixel basis. Hence, we may assume blind inversion imaging problem to be space-variant. 2D Cauchy Machine is employed as a Fast Simulated Annealing (FSA) algorithm to find an unknown de-mixing matrix associated with the global minimum of the Helmholtz free energy while MaxEnt like algorithm is used to find the distribution of the source vector with the maximal entropy under given macroscopic constraints defined by data vector itself [3,4].

Brief description of the blind space-variant imaging problem is given in Section II while more details can be found in [5]. Section III describes application of the 2D version of the FSA algorithm based on the Cauchy Machine theory, [3,4], on the blind space-variant imaging problem. In Section IV we demonstrate capability of the 2D Cauchy Machine to find the global minimum of the very difficult 'golf hole' type of landscape. Performance comparison in terms of computational complexity in relation to the exhaustive search approach is also given in Section IV. Here we also demonstrate the algorithm capability to perfectly recover images from the synthetic noise free linear mixture of two images. Conclusion is given in Section V.

II. BLIND SPACE-VARIANT IMAGING PROBLEM

Data model for blind space-variant imaging problem is defined with:

$$\vec{X}_{(p,q)} = [A]_{(p,q)}\vec{S}_{(p,q)} \tag{1}$$

where $\vec{X}$ and $\vec{S}$ are n and m dimensional column vectors of integers representing measured data and unknown sources respectively with $m \le n$ and [A] being nxm unknown mixing matrix. The subscript (p,q) denotes spatial coordinates i.e. the blind imaging problem is formulated on the pixel by pixel basis. Note that such formulation allows the mixing matrix $[A]_{(p,q)}$ to be spatially variant. The goal of the blind inversion imaging algorithms is to find both the unknown source vector $\vec{S}$ and an unknown mixing matrix [A] based on data vector $\vec{X}$ only. We shall drop (p,q) subscript in the subsequent derivations in order to simplify notation. Because both $\vec{X}$ and $\vec{S}$ have the physical interpretation of intensity the positivity constraint is imposed on them:

$$\begin{aligned} x_i &\ge 0 \quad i = 1,\ldots,n \\ s_i &\ge 0 \quad i = 1,\ldots,m \end{aligned} \tag{2}$$

If the unknown mixing matrix has physical interpretation of the spectral reflectance matrix as in remote sensing, [5,6], or point spread function of the optical or non-optical imaging system than positivity constraints must be imposed on [A] too:

$$a_{ij} \ge 0 \;\; i = 1,..,n;\; j = 1,..,m \tag{3}$$

We shall rewrite (1) in a slightly different form:

$$\vec{X} = [A]N\vec{S}' \tag{4}$$

where:

$$N = \sum_{i=1}^{m} s_i \qquad s_i' = \frac{s_i}{N} \tag{5}$$

With (4) we have introduced unknown magnitude of the source vector N that helped us to assign to the components of the scaled source vector $\vec{S}'$ the meaning of probability because due to (5) they satisfy the constraint:

$$\sum_{i=1}^{m} s_i' = 1 \tag{6}$$

Solution of deterministic blind space-variant imaging problem (1) is given by finding unknown de-mixing matrix $[W] \cong [A]^{-1}$ and unknown source vector $\vec{S}$ based on the data vector $\vec{X}$ only on the pixel-by-pixel basis. Feed-forward type of the Lagrange constraint neural network shown on Figure 2, [5,7] is employed to find the unknown source vector $\vec{S}$ and 2D Cauchy Machine [3,4] is used to find the uknown de-mixing matrix [W] at the global minimum of the 'golf hole' type of landscape associated with the Helmholtz free energy:

$$\begin{aligned} \left([W^*], N^*\right) &= \arg\min|H| \cong \arg\min|U| \\ &= \arg\min\left([W]\vec{X} - N\vec{S}'\right)^T\left([W]\vec{X} - N\vec{S}'\right) \end{aligned} \tag{7}$$

where Helmholtz free energy is defined with:

$$\begin{aligned} H([W],\vec{S}) &= U - T_0 S \\ &= \vec{\mu}^T\left[[W]\vec{X} - N\vec{S}'\right] + K_B T_0 N \sum_{i=1}^{m} s_i' \ln s_i' \\ &\quad + N(\mu_0 - K_B T_0)\left(\sum_{i=1}^{m} s_i' - 1\right) \end{aligned} \tag{8}$$

and Shannon entropy was approximated by:

$$S = -K_B T_0 \sum_{i=1}^{m} s_i' \ln s_i' \tag{9}$$

where K_B represents Boltzmann's constant and T_0 represents temperature. They are introduced in (8) due to dimensionality reasons. Equivalence in minimization of H and U w.r.t. [W] and N (7) is due to the fact that Shannon entropy S in (8) does not depend on [W] and N. Minimization of the objective function (7) gives as a solution distribution $p(\vec{S})$ with the maximal entropy under given macroscopic constraints $U = \left([W]\vec{X} - N\vec{S}'\right)$ defined by measured data $\vec{X}$:

$$\sum_{i=1}^{n} w_{ji} x_i = N s_j' \tag{10}$$

FSA algorithm based on Cauchy Machine looks for the global minimum of the Helmholtz free energy (7)/(8) to find the unknown de-mixing matrix while MaxEnt like algorithm is used to find the most probable distribution $p(\vec{S}) = \vec{S}'$ for a given doublet $\left([W^{(l)}], N^{(l)}\right)$ where l denotes iteration index in a solution of problem (7). Probability of the unknown source vector is obtained at the thermodynamic equilibrium i.e. minimum of the Helmholtz free energy (8) as, [5,7]:

$$s_j' = \frac{1}{1 + \sum_{\substack{i=1 \\ i \ne j}}^{m} \exp\left(\frac{1}{K_B T_0}\left(\mu_i - \mu_j\right)\right)} = \sigma(\vec{\mu}) \tag{11}$$

Lagrange multipliers, that have interpretation of virtual sources, are updated as [5]:

$$\mu_j^{(k+1)} = \mu_j^{(k)} + \left(\frac{K_B T_0}{s_j^{,(k)}} + \mu_j^{(k)} \right) \left(\vec{w}_j^{(l)} \vec{X} - N^{(l)} s_j^{,(k)} \right) + \sum_{\substack{i=1 \\ i \neq j}}^{m} \mu_i^{(k)} \left(\vec{w}_i^{(l)} \vec{X} - N^{(l)} s_i^{,(k)} \right) \quad (12)$$

where k stands for iteration index related to the Lagrange multipliers learning rule and l stands for the iteration index related to the iterative solution of the optimization problem (7).

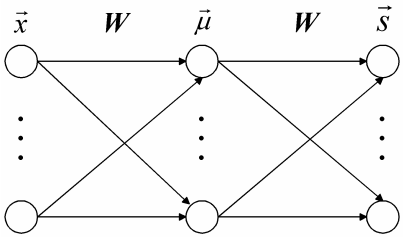

Figure 2. A Feed-forward Lagrange Constraint Neural Network, [7,5].

At some iteration l output doublet $\left([W]^{(l)}, N^{(l)} \right)$ is generated as an output of the Cauchy Machine based FSA optimization algorithm in an attempt to reach possibly global minimum of the estimation error energy (7). For a given doublet $\left([W]^{(l)}, N^{(l)} \right)$ the MaxEnt like algorithm (11)-(12) computes the most probable solution for the source vector $\vec{S}^{(l)} = N^{(l)} \vec{S}^{,(l)}$. This represents feedback for the Cauchy Machine algorithm that computes a new value of the estimation error energy and generates a new doublet $\left([W]^{(l+1)}, N^{(l+1)} \right)$. After each iteration l is completed we get a triplet $\left([W]^{(l)}, N^{(l)}, \vec{S}^{,(l)} \right)$. Algorithm accepts as a final solution the triplet $\left([W]^{*}, N^{*}, \vec{S}^{,*} \right)$ for which the estimation error energy (7) reaches a possibly global minimum

III. CAUCHY MACHINE SIMULATED ANNEALING ALGORITHM FOR BLIND SPACE-VARIANT IMAGING PROBLEM

As in [5,6] we model 2D space-variant imaging problem by using two mixing angles θ and φ:

$$\begin{bmatrix} x_x \\ x_y \end{bmatrix} = N \begin{bmatrix} \cos\theta & \cos\varphi \\ \sin\theta & \sin\varphi \end{bmatrix} \begin{bmatrix} s'_x \\ s'_y \end{bmatrix} \quad (13)$$

Based on (13) the unknown de-mixing matrix [W] is described by two 'killing' angles ξ and ζ as [5]:

$$[W] = \frac{1}{\sin(\zeta - \xi)} \begin{bmatrix} \cos\xi & \sin\xi \\ \cos\zeta & \sin\zeta \end{bmatrix} = \begin{bmatrix} \vec{w}_1 \\ \vec{w}_2 \end{bmatrix} \quad (14)$$

Vector diagram representation of the mixing model (3)/(13)/(14) is shown on Figure 3. The unknown de-mixing matrix [W] is found at a global minimum of the Helmholtz free energy objective function (7)/(8) using FSA based on 2D Cauchy Machine. Therefore a 2D Cauchy probability density function (pdf) in the killing angles domain is defined [3,4]:

$$p(\varsigma, \xi) = \frac{K_1}{K_2} \frac{c}{\left| \varsigma^2 + \xi^2 + c^2 \right|^{3/2}} \quad (15)$$

where K_1 and K_2 are normalization constants to be determined. Due to the positivity constraints (3) the killing angles lie in the domain:

$$\varsigma \in \left[\frac{\pi}{2}, \pi \right] \quad \xi \in \left[-\frac{\pi}{2}, 0 \right] \quad (16)$$

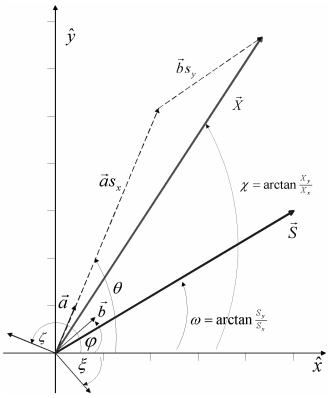

Figure 3. Vector diagram representation of the mixing model (3)/(13)/(14).

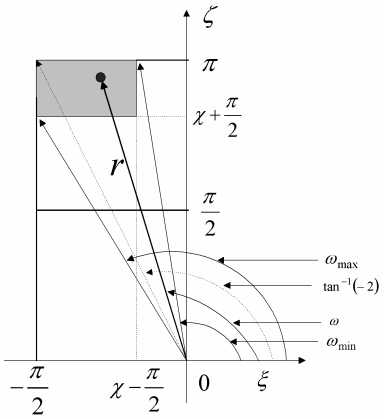

Figure 4 Geometry relations between Cartesian (ξ, ζ) and polar (r, ω) coordinates.

If, based on Figure 3, we adopt the convention that for original mixing angles θ and φ it applies the following:

$$\varphi \leq \chi \leq \theta \quad (17)$$

where χ is angle defined by data vector $\vec{X}$ as:

$$\chi = \tan^{-1}\left(\frac{x_x}{x_y}\right) \tag{18}$$

than domain of support for killing angles is narrowed according to:

$$\varsigma \in \left[\frac{\pi}{2}+\chi, \pi\right] \quad \xi \in \left[-\frac{\pi}{2}, -\frac{\pi}{2}+\chi\right] \tag{19}$$

which reduces the size of the search space. The 2D pdf (15) can be transformed from the Cartesian $p(\zeta,\xi)$ to polar $p(r,\omega)$ coordinates using standard transformation from Cartesian to polar coordinate system. Due to (19) the angle polar coordinate ω lies in:

$$\omega_{\min} \le \omega \le \omega_{\max} \tag{20}$$

where ω_{min} and ω_{max} are defined with:

$$\omega_{\max} = \tan^{-1}\frac{\chi+\pi/2}{-\pi/2} \qquad \omega_{\min} = \tan^{-1}\frac{\pi}{\chi-\pi/2} \tag{21}$$

The radial coordinate *r* lies in:

$$r \in [r_{\min}, r_{\max}] \tag{22}$$

where r_{min} and r_{max} are given for a particular value of ω with:

$$r_{\min} = \frac{\chi+\pi/2}{\sin\omega}$$

$$r_{\max} = \begin{cases} \dfrac{\pi}{\sin\omega} & \omega \in [\omega_{\min}, \pi+\tan^{-1}(-2)] \\ -\dfrac{\pi}{2\cos\omega} & \omega \in [\pi+\tan^{-1}(-2), \omega_{\max}] \end{cases} \tag{23}$$

Geometry relations between Cartesian (ξ,ζ) and polar (r,θ) coordinate systems are illustrated on Figure 4. Cartesian pdf $p(\zeta,\xi)$ (15) can be written in polar coordinates $p(r,\omega)$ as:

$$p(r,\omega) = p(\omega)p(r) = K_1 K_2 \frac{cr}{\left(r^2+c^2\right)^{3/2}} \tag{24}$$

Pdf $p(\omega) = K_1$ is determined from the requirement:

$$\int_{\omega_{\min}}^{\omega_{\max}} p(\omega)d\omega = 1 \tag{25}$$

from which it follows:

$$p(\omega) = K_1 = \frac{1}{\omega_{\max}-\omega_{\min}} \tag{26}$$

Normalization constant K_2 is determined from the requirement:

$$\int_{r_{\min}}^{r_{\max}} \frac{1}{K_2}\frac{cr}{\left(r^2+c^2\right)^{3/2}}dr = 1 \tag{27}$$

from which it follows:

$$K_2 = c\left(\frac{1}{\sqrt{r_{\min}^2+c^2}} - \frac{1}{\sqrt{r_{\max}^2+c^2}}\right) \tag{28}$$

and also:

$$p(r) = \frac{c}{K_2}\frac{r}{\left(r^2+c^2\right)^{3/2}} \tag{29}$$

Both distributions $p(\omega)$ and $p(r)$ have to be generated from the uniform distribution with the domain of support on $[0,1]$ interval. The guiding principle for designing generation law is:

$$|p(\omega)d\omega| = |p(x)dx| \tag{30}$$

and:

$$|p(r)dr| = |p(x)dx| \tag{31}$$

where *x* is random variable uniformly distributed on the interval $[0,1]$. It follows from (30):

$$p(\omega) = p(x)\frac{dx}{d\omega} = \frac{1}{\omega_{\max}-\omega_{\min}} \tag{32}$$

because *p(x)=1*. It follows from (32):

$$x = \int p(\omega)d\omega = \frac{1}{(\omega_{\max}-\omega_{\min})}\omega + C_0 \tag{33}$$

We get from (33):

$$\omega = (\omega_{\max}-\omega_{\min})x + \overline{C}_0 \tag{34}$$

where integration constant $\overline{C}_0$ is determined from the boundary conditions that for $x \in [0,1] \Rightarrow \omega \in [\omega_{\min}, \omega_{\max}]$ which gives :

$$\omega = (\omega_{\max}-\omega_{\min})x + \omega_{\min} \tag{35}$$

which is transformation law required for generating random variable ω uniformly distributed in the interval $[\omega_{\min}, \omega_{\max}]$. To find the transformation law for random variable *r* we have to derive relation between uniformly distributed variable *x* and random variable *r* the pdf of which is given by (29). It follows from (31):

$$p(r) = p(x)\frac{dx}{dr} \tag{36}$$

where *x* is uniformly distributed on some interval [x_{min},x_{max}] and from (36):

$$x = \int p(r)dr = -\frac{c}{K_2}\frac{1}{\sqrt{r^2+c^2}} \tag{37}$$

Here *p(x)=const.* is absorbed into K_2 in (37). It follows from (37):

$$r = \frac{c}{K_2 x}\sqrt{1-K_2^2x^2} \tag{38}$$

In (38) *x* is uniformly distributed on the interval [x_{min}, x_{max}] such that:

$$r(x_{\min}) = r_{\min} \quad r(x_{\max}) = r_{\max} \tag{39}$$

It follows from (38) and (39):

$$x_{\min} = \frac{1}{K_2\sqrt{1+r_{\min}^2}} \quad x_{\max} = \frac{1}{K_2\sqrt{1+r_{\max}^2}} \tag{40}$$

Relation between random variable *x* uniformly distributed on the interval [x_{min}, x_{max}] and random variable $\tilde{x}$ uniformly distributed on the interval [0, 1] is given through:

$$x=(x_{\max}-x_{\min})\tilde{x}+x_{\min} \quad (41)$$

Like in Boltzmann Machine based simulated annealing algorithm [1] the new solution in terms of killing angles (ξ,ζ) at some iteration *k* is accepted if either:

$$|H(k)|<|H(k-1)| \quad (42)$$

or if Metropolis criteria [1] is satisfied:

$$p_k \le \frac{1}{(1+e^{\Delta E_k/T})} \quad (43)$$

where p_k is uniformly generated probability and $\Delta E_k=|H(k)|-|H(k-1)|$ is error energy at iteration *k*. Metropolis criteria (43) avoids algorithm to escape from local minima even if value of the Helmholtz free energy at iteration *k* is greater than value at the previous iteration.

IV. SIMULATION RESULTS

We illustrate application of the 2D Cauchy Machine algorithm on the 2D case of Eq.(4) given by (13). Un-mixing matrix [*W*] is given by (14) where angles ξ,ζ are related to the angles θ,φ through, Figure 3:

$$\xi=\varphi-\frac{\pi}{2}\ \ \zeta=\theta+\frac{\pi}{2} \quad (44)$$

If according to (13) we choose $\theta=64^0,\varphi=45^0$, N=*8*,s_1=*5*,s_2=*3* Eq.(13) becomes:

$$\begin{bmatrix}4.3132\\6.6153\end{bmatrix}=8x\begin{bmatrix}0.4384 & 0.7071\\0.8988 & 0.7071\end{bmatrix}\begin{bmatrix}0.6250\\0.3750\end{bmatrix} \quad (45)$$

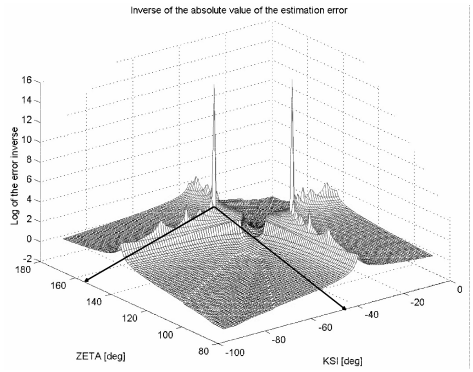

Figure 5. 2D plot of the log of inverse of (7) in the angle domain. Note two very sharp peaks that according to (44) give two solutions $\xi^1=-45^0,\zeta^1=154^0$ and $\xi^2=-26^0,\zeta^2=135^0$.

Figure 5 shows log of the inverse of the error energy function (7) as a function of angles ξ,ζ for given values of *N=8*,s_x=*5*,s_y=*3*. Note two very sharp peaks that according to (44) correspond two solutions $\xi^1=-45^0,\zeta^1=154^0$ and $\xi^2=-26^0,\zeta^2=135^0$. Two solutions are consequence of the non-unique representation of data vector (13) i.e.:

$$\vec{X}=N(\vec{a}s_x'+\vec{b}s_y')=N(\vec{b}s_y'+\vec{a}s_x') \quad (46)$$

From the single pixel point of view this permutation is not a problem. From the space variant imaging point of view it could create problems because related components of two different source vectors corresponding with two different pixels could be assigned on two different images. If, based on vector diagram on Figure 3, we adopt convention (17) this type of permutation indeterminacy can be resolved for the space-variant case. Figure 6 shows number of iteration necessary for 2D Cauchy Machine algorithm (15)-(43) to find global minimum of the 'golf hole' type of error energy function (7) for 100 runs. Solid line on Figure 6 represents fixed number of iteration required by exhaustive search algorithm that in this example is 1972. The average number of iteration per run using 2D Cauchy simulated annealing algorithm was 1684 while exhaustive search required 1972 iterations to find solution. This gives an estimate of the speed-up factor as 1972/1684≈1.171 or 17%.

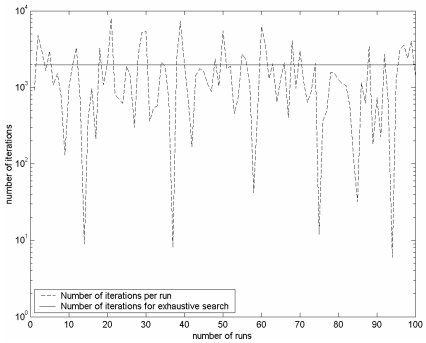

Figure 6. Number of iterations per run for overall 100 runs necessary to find global minimum of the error energy function (7) by using 2D Cauchy Machine FSA algorithm (15)-(43) (dashed line) and exhaustive search algorithm (solid line).

We now mix two images by a mixing matrix that has been changed from pixel to pixel in order to simulate the space variant imaging problem. Angles θ and φ are changed column wise according to Figure 7 i.e. for every column index angles were changed for 1^0 and mutual distance between them was 4^0. Figure 8 shows from left to right two source images, two mixed images, two separated images using 2D Cauchy Machine blind inversion algorithm (7)-(43) and two separated images using Infomax ICA algorithm, [9]. Thanks to the fact that Cauchy Machine blind inversion algorithm solves the problem on the pixel-by-pixel basis the recovery was perfect although mixing matrix was space variant. Due to the space variant nature of the mixing matrix Infomax algorithm failed to recover the original images.

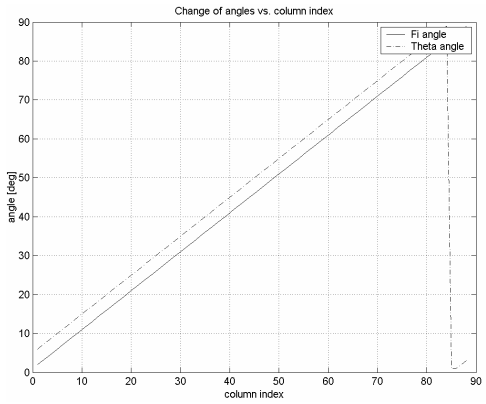

Figure 7. Change of the angles vs. column index . Solid line - φ angle; dashed line - θ angle.

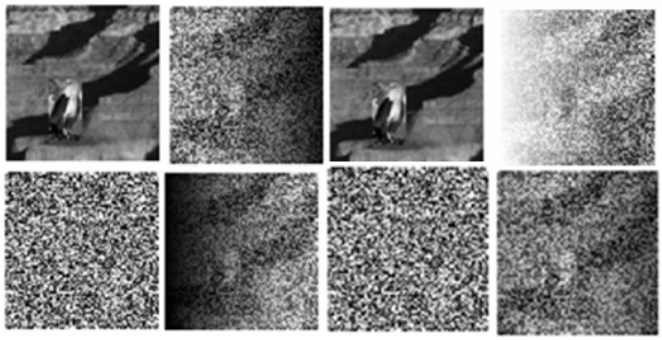

Figure 8. From left to right are: source images; space variant noise free mixture; error free recovery of the source images using 2D Cauchy Machine blind inversion algorithm (7)-(42), recovery of the source images using ICA Infomax algorithm [9].

V. CONCLUSION

A 2D Cauchy machine capable of solving space-variant imaging problem on the pixel-by-pixel basis has been presented. This is accomplished by minimization of the Helmholtz free energy as an objective function. It has been demonstrated that Helmholtz free energy has stable global minimum in the domain of support of the un-mixing matrix. Because of the 'golf hole' type of landscape of this objective function it is almost impossible to reach it by means of the gradient descent algorithms. It has been demonstrated that 2D Cauchy machine is capable to find a global minimum in such a difficult landscape under significantly less computational time than exhaustive search technique. Performance of blind inversion algorithm based on 2D Cauchy Machine has been demonstrated on the perfect recovery of images from the synthetic noise free space-variant linear mixture of two images. Due to the space-variant nature of the mixture ICA algorithms fail to recover unknown source images.

REFERENCES

1. Ackley, D.H., Hinton, G.E. and Sejnowski, T.J, "*A learning algorithm for Boltzman Machines*", Cognitive Science 9, 147-169, 1985.
2. S. Geman and D. Geman, "*Stochastic relaxation, Gibbs distribution and the Bayesian restoration of images*," IEEE Transactions on Pattern Analysis and Machine Intelligence, vol. PAMI-6, no. 6, pp. 721-741, November 1984.
3. H. Szu and R. Hartley, "Nonconvex Optimization by Simulated Annealing," *Proc. IEEE*, 75, No. 11, 1987, 1538-1540.
4. H. Szu and R. Hartley, "Fast Simulated Annealing," *Physics Letters A*, 122, No. 3, 1987, 157-162.
5. H. Szu and I. Kopriva, "Deterministic Blind Source Separation for Space Variant Imaging," Fourth International Symposium on Independent Component Analysis and Blind Signal Separation, Nara, Japan, April 1-4, 2003.
6. I. Kopriva and H. Szu, "Deterministic Blind Source Separation for Space Variant Imaging with Sensor Nonlinearities," SPIE AeroSense Symposium – Independent Component Analysis, Wavelets and Neural Networks, Orlando, FL, April 22-25, 2003.
7. H.H.Szu and I.Kopriva, "Comparison of the Lagrange Constrained Neural Network with Traditional ICA Methods," Proc. of the 2002 World Congress on Computational Intelligence-International Joint Conference on Neural Networks, pp. 466-471, Hawaii, USA, May 17-22, 2002.
8. S. Amari, A. Cihocki, H. H. Yang, "A new learning algorithm for blind signal separation," *Advances in Neural Information Processing Systems*, **8**, MIT Press, 757-763, 1996.
9. A. J. Bell and T. J. Sejnowski, "An information-maximization approach to blind separation and blind deconvolution," *Neural Comp.* **7**, 1129-1159 , 1995.
10. A. Hyvärinen and E. Oja, "A fast fixed-point algorithm for independent component analysis," *Neural Computation*, vol. 9, pp. 1483-1492, 1997.